

LASER INTERFEROMETER GRAVITATIONAL WAVE OBSERVATORY
- LIGO -
CALIFORNIA INSTITUTE OF TECHNOLOGY
MASSACHUSETTS INSTITUTE OF TECHNOLOGY

Technical Note	LIGO-T1600064-v2	2016/03/16
<h1>ISS second loop requirements</h1>		
Gabriele Vajente		

Distribution of this document:
LIGO Scientific Collaboration

Draft

California Institute of Technology
LIGO Project, MS 18-34
Pasadena, CA 91125
Phone (626) 395-2129
Fax (626) 304-9834
E-mail: info@ligo.caltech.edu

Massachusetts Institute of Technology
LIGO Project, Room NW17-161
Cambridge, MA 02139
Phone (617) 253-4824
Fax (617) 253-7014
E-mail: info@ligo.mit.edu

LIGO Hanford Observatory
Route 10, Mile Marker 2
Richland, WA 99352
Phone (509) 372-8106
Fax (509) 372-8137
E-mail: info@ligo.caltech.edu

LIGO Livingston Observatory
19100 LIGO Lane
Livingston, LA 70754
Phone (225) 686-3100
Fax (225) 686-7189
E-mail: info@ligo.caltech.edu

1 Scope of this document

In this document we revise the design requirements for the intensity stabilization servo (ISS) second loop system.

In section 2 we review the measured performance of the ISS second loop system as installed now, and compare it with the requirements from the design document. We also compare those requirements with the results from optical simulations carried out with different input powers and residual thermal lensing in the ITM substrates.

In section 3 we discuss the present design of the transimpedance electronics, and describe the functional and noise requirements that can be derived from the RIN requirements and from the experience gained during the commissioning of the ISS second loop system.

In section 4 we describe the required performance of the second loop servo electronics to meet the RIN requirements stated above, and compare with the present system. We derive the servo gain, as a function of frequency, that is needed, and discuss additional functional requirements based on the ISS commissioning experience.

2 RIN requirements

2.1 Current performance

The in-vacuum array of 8 photodiodes and one quadrant is installed and functional at LHO. Figure 1 shows the measured performance of the installed system with a power of 22 W into the IFO. The blue trace shows the RIN of the beam transmitted by the IMC when the second loop is open, as measured on the ISS array photodiodes (sum of four).

This level of noise can change significantly with the alignment state of the IMC. In particular this data was taken in a not very good alignment condition for the IMC. Figure 2 (from [13]) shows that by optimizing the IMC angular control offsets it is possible to get rid of most of the structures above about 100 Hz in the open-loop RIN.

When the second loop is closed on the sum of four diode, the in-loop signal (orange trace) is reduced by the loop gain, while the out-of-loop signal (yellow trace), as expected, shows a much lower reduction. The out-of-loop signal is expected to be limited by sensor noise (either in the in-loop or out-of-loop signals). The green trace shows the level corresponding to the shot noise (considering the quadrature sum of the in-loop shot noise and the out-of-loop shot noise). Above 100 Hz, the out-of-loop RIN is quite close to the expected shot noise ($7 \times 10^{-9}/\sqrt{\text{Hz}}$ instead of $5.8 \times 10^{-9}/\sqrt{\text{Hz}}$). However, at frequencies below 100 Hz the measured residual RIN is significantly larger than the shot noise. The origin of this discrepancy is not understood yet. During the one hour of data used for this spectrum, the noise below 100 Hz was stationary. Possible origins to

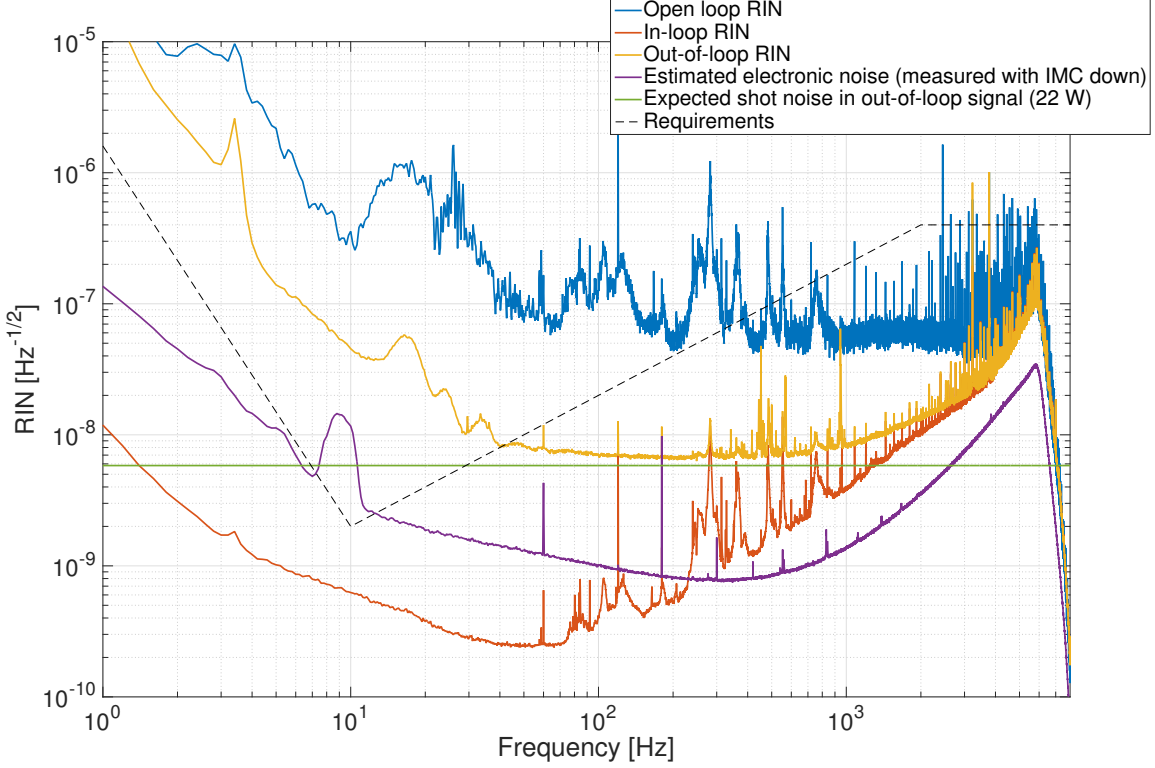


Figure 1: Measured performance of the LHO ISS second loop, with a power of 22 W into the IFO. The blue trace is the measured RIN at the in-vacuum array, when the second loop is open, but the first loop is closed. The yellow and orange traces shows the out-of-loop and in-loop RIN when the second loop is closed. The green trace shows the expected shot noise level in the out-of-loop signal. The purple trace is an estimate of the total electronic noise, i.e. the signal when no light is impinging on the diodes. Finally, the dashed black line is the RIN requirement from the ISS design document [1].

be investigated are:

- scattered light due to a spurious beam entering the array;
- beam jitter noise due to non optimal centering of the beam on the PDs;
- artifact due to the way the RIN is computed, which is dividing the whitened PD signals by a low passed monitor signal of the DC power impinging on the diode. Fake noise in the RIN has been seen in the past [7]. The raw signals out of the diodes are available in the online frames but not written to disk, so we couldn't check if this is the case.

This additional low frequency noise is a very important issue that must be tackled, since it might be a fundamental limit on the ISS performance. There is no evidence that this is an issue related to the electronics.

The purple trace in fig. 1 shows an estimate of the electronic noise. This curve was taken with the

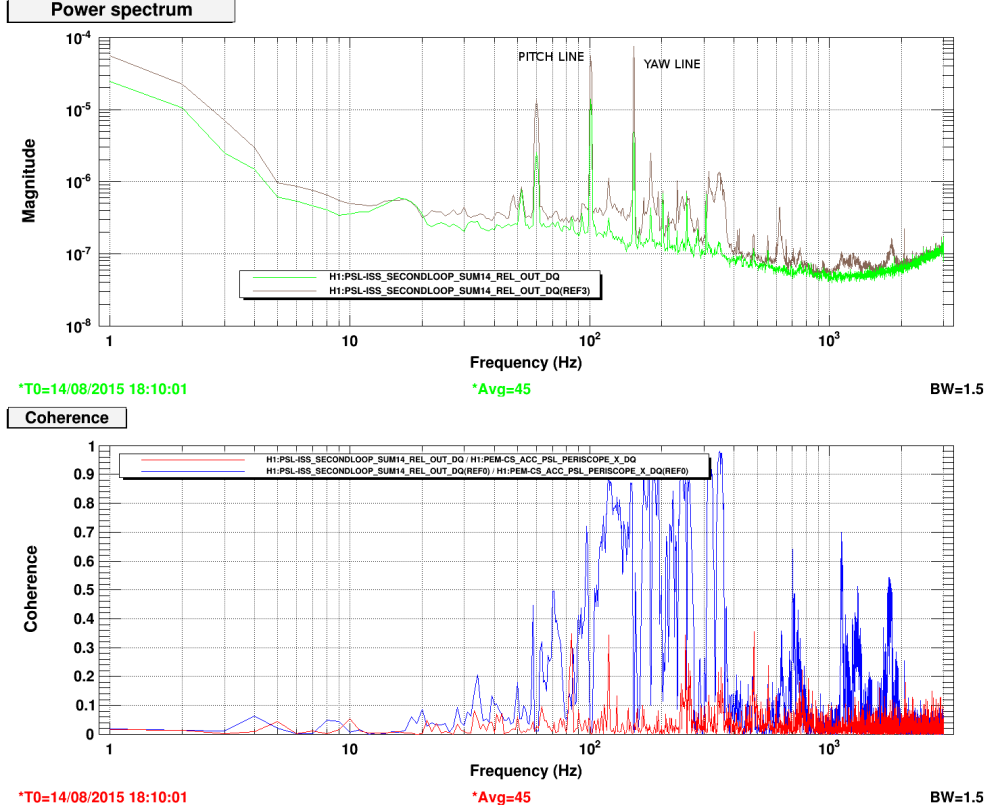


Figure 2: Impact of the IMC alignment on the RIN in transmission. Top panel: the brown trace shows the RIN with a poor alignment, the green trace with the improved alignment. Bottom panel: coherence between the IMC transmitted RIN and input beam jitter, blue with poor alignment, red with the improved alignment. Plot from [13].

IMC not locked (so some residual light flashed might have been present and could explain the peak at 10 Hz) and a power of 2.2 W. The noise has been rescaled to the RIN corresponding to 22 W. This level of electronic noise is slightly above the requirements at 10 Hz, but one should consider that it will scale down proportionally to the input power.

Finally, the dashed curve shows the RIN requirement as obtained from the ISS design document [1].

2.2 Simulation of RIN requirements

To cross check the RIN requirements considered above, we ran an optical simulation based on MIST [8]. For different IFO input powers between 25 and 125 W, we computed the coupling of laser intensity noise at the IFO input to the differential arm signal (DARM), including radiation pressure effects. For each input power we also computed the expected sensitivity using GWINC [9]. We then computed the maximum allowed input RIN by requiring that the noise contribution to DARM is lower than 1/10 of the sensitivity. The results are shown in fig. 3.

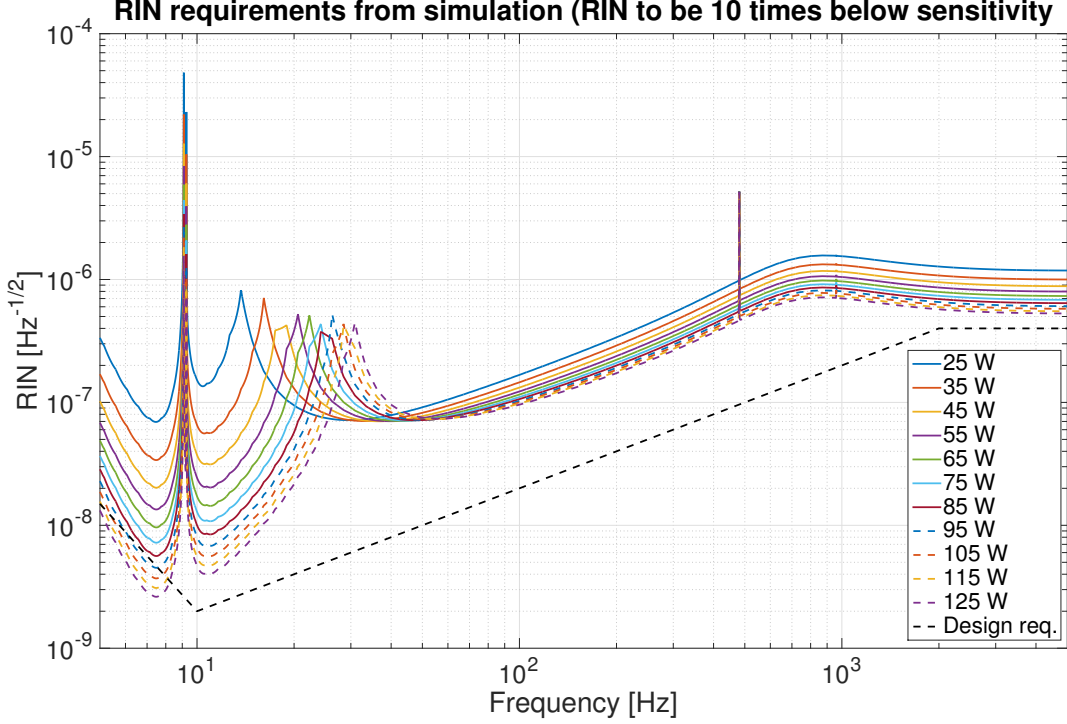


Figure 3: Simulated (with MIST and GWINC) requirements on the RIN at the interferometer input, for different input powers. The IFO is ideal (no spurious asymmetries, such as thermal lensing in the ITM substrates or mis-match of cavities) and the simulation include radiation pressure effects. The black dashed line shows the requirements from the ISS design document [1].

The simulated requirements are systematically above the one quoted in the ISS second loop design document [1], so we can safely continue to use the latter for computations at full power. When operating at lower powers, the high frequency region (above 40 Hz) does not change more than a factor of 2. The low frequency requirement (below 30 Hz) instead changes a lot, as expected since this frequency region is dominated by radiation pressure coupling.

Measurements done at LHO showed that the coupling of intensity noise, at frequencies above few hundred Hz, can be much larger than expected [10]. It was later understood, with simulation [11] that the increased coupling is due to a differential residual lensing in the ITM substrates. Once the TCS system was tuned to compensate for this, the coupling of RIN to DARM was reduced to a level qualitatively compatible with simulations in the ideal case [12]. The result reported there is shown in fig. 4. The green dots are the measured coupling from RIN at the IFO input to the DCPD signal, when the ITM substrate lensing was poorly compensated. The blue trace shows the same transfer function after a tuning of the TCS system. This trace can be compared with the red trace, which is the result of a simulation (not the same as shown above).

Figure 5 shows a similar, more recent, measurement done at LHO, this time calibrated in DARM displacement over RIN at the IFO input. The various lines in the same plot show the result of optical simulations, with different values of the differential lensing in the ITM substrates. The result of the simulations are in qualitative agreement with the measurement, and as before the

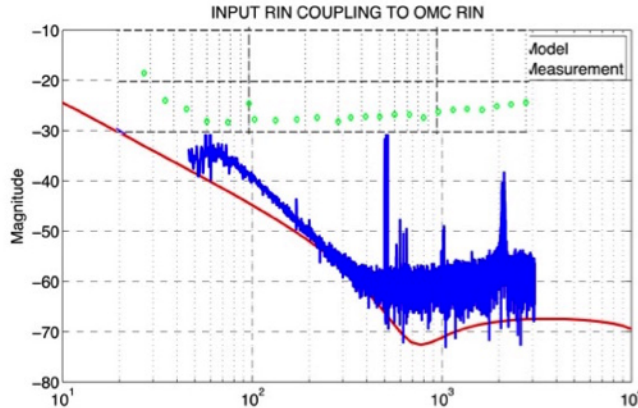


Figure 4: Plot from [10]. Measured coupling of RIN at the IFO input to DCPD signal. The green markers show a measurement with poorly compensated ITM lensing. The blue curve shows the same coupling when the TCS system was optimized. The read trace is a simulation of the coupling in a ideal case. Blue and red curves are close. NOTE: Commissioners at LHO are planning to repeat this kind of measurement, by taking the RIN transfer function for different TCS set points. We will get transfer functions calibrated in DARM/RIN that we will compare with the simulations done above.

increased coupling at high frequency can be ascribed to a poor compensation of the ITM substrate lensing. Tests are planned to improve the compensation and see if the RIN coupling decreases. However, noise projections at 22 W show that laser intensity noise is well below the measured sensitivity at all frequencies [15]. The measured transfer function is significantly larger than what is expected from simulation, at frequencies below 20 Hz. The reason has not been investigated so far, but it seems unlikely to be related to a larger than expected radiation pressure coupling.

We can conclude that the observed increase of RIN coupling is well understood and that we have a strategy to cope with it, so there is no evidence that we need to tighten the requirements.

3 Transimpedance electronics

The current transimpedance electronics is described in [5]. Each board provides the bias and the readout for four diodes. The original outputs were whitened single diode channels to be readout by ADCs, a sum of the four whitened signals to be sent to the second loop servi board, and a monitoring output for the same sum. During the on site alignment of the array, it turned out that the whitening was too aggressive at DC, making it impossible to reconstruct the DC power impinging on each diode. Therefore some temporary monitoring outputs were added, picking up the signal right after the transimpedance amplifier and before the whitening circuit.

We propose the following changes of the transimpedance electronics architectures, shown schematically in fig. 6:

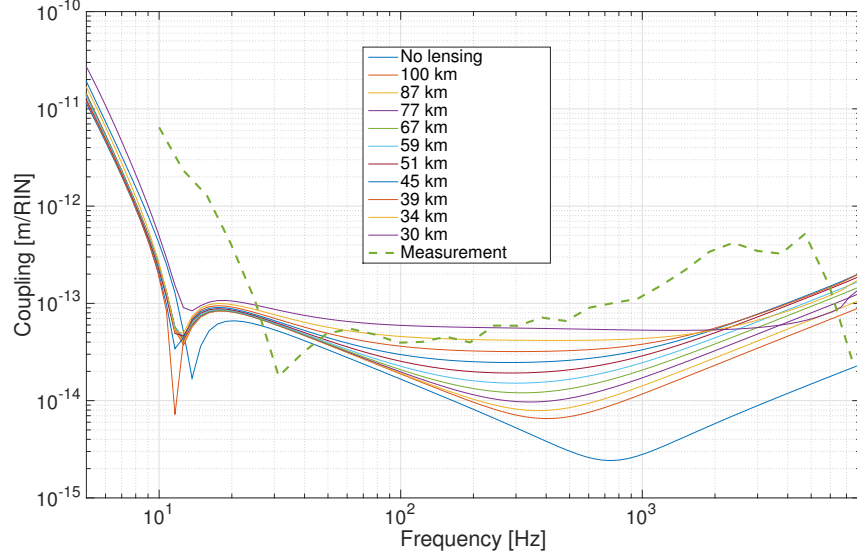


Figure 5: Measurement of RIN coupling to DARM at LHO (green dashed line). The thin lines show simulation results for different values of the differential focal length in the ITM substrates.

- Add four monitoring channels of the output of each transimpedance amplifier, to be sent un-whitened to slow monitoring ADCs
- Move the whitening to four fast monitoring channels, one for each photodiode. The current whitening is sufficient, as shown by the electronic noise curve of fig. 1
- Do not add any whitening in the sum servo path. With this change all the loop shaping will be done in the servo board. Presently the servo add low frequency boosts, partly to compensate for the whitening filter. We think it's more logical to apply whitening only when needed for digital acquisition.
- Add a monitoring channel for the sum, with the same whitening as the single PD channels
- In the current electronics, all monitoring channels are single ended. We might consider changing to differential.

Presently the transimpedance electronics is on the floor below the chamber, to reduce to a minimum the length of the cables going from the PDs to the electronics. It would be more practical to move the electronics on the PSL rack. We should consider if this is possible, taking into account the cable length and possible compensations for the added capacitance.

The power into the ISS array is 0.2% of the power to the IFO input. Of this only 0.5% goes to the QPD. Therefore at the present power of 22 W, we have 44 mW total at the array input, divided among the eight diodes: 5.5 mW per diode, corresponding to a photocurrent of 4.1 mA (assuming a responsivity of 0.75 A/W). At full power we'll have 250 mW total into the array, corresponding to 31.3 mW per diode, or a photocurrent of 23.4 mA. If we want to use optimally the entire 15V range of the electronics at full power, the transimpedance should be 640 Ω . A slightly larger value,

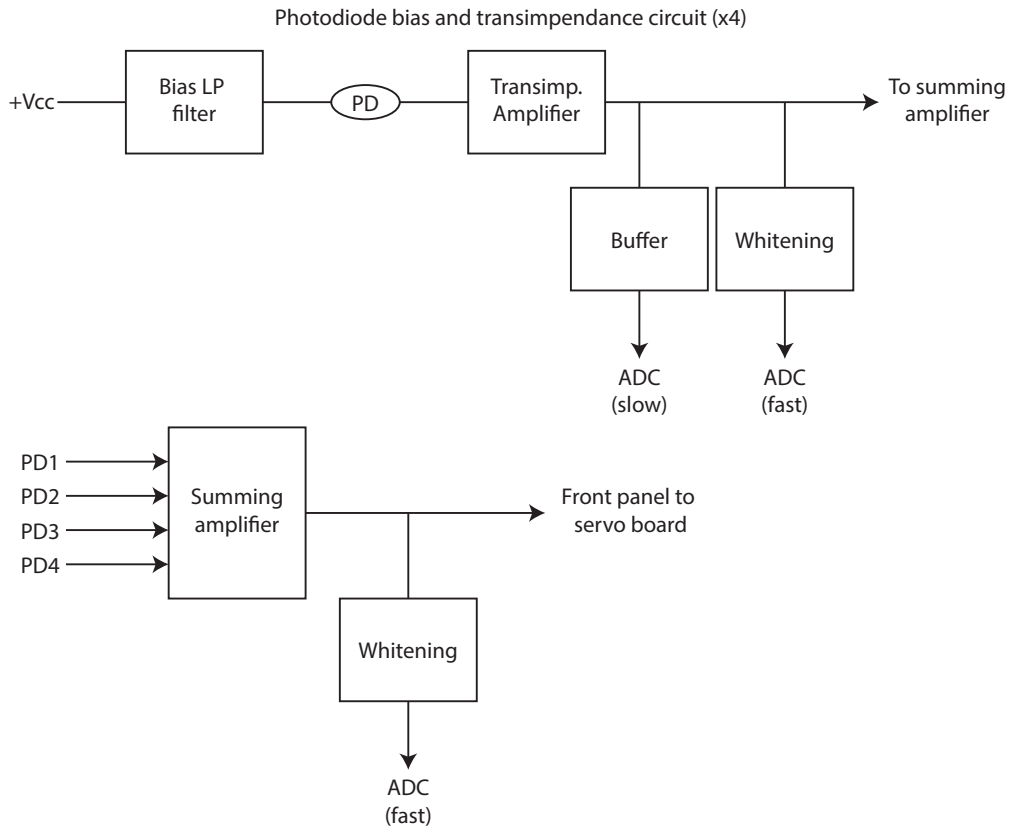


Figure 6: Block diagram of the proposed transimpedance electronics.

like $1\text{ k}\Omega$ would be advisable to have some margin. For comparison, the current electronics has a transimpedance of $1.62\text{ k}\Omega$ [5].

The limit noise source for the ISS second loop performance would ultimately be shot noise. For 22 W input power, each diode will be limited by a shot noise of $4.6 \times 10^{-11} \text{ W}/\sqrt{\text{Hz}}$ or $3.5 \times 10^{-11} \text{ A}/\sqrt{\text{Hz}}$. At full 125 W input power, we have $1.1 \times 10^{-10} \text{ W}/\sqrt{\text{Hz}}$ or $8.3 \times 10^{-11} \text{ A}/\sqrt{\text{Hz}}$. The electronic noise of the transimpedance, referred to the input, should be significantly lower than the shot noise level for 22 W input power, which is the most stringent.

4 Second loop servo

4.1 RIN suppression requirements

We can derive a requirement on the ISS second open loop gain from the ratio of the measured noise (with ISS second loop open), and the RIN requirement. The result is shown in the blue trace in fig. 7. The orange trace is the proposed open loop gain of the second loop, to include some margin. The unity gain frequency is around 1 kHz , and the gain at 10 Hz is about 500 .

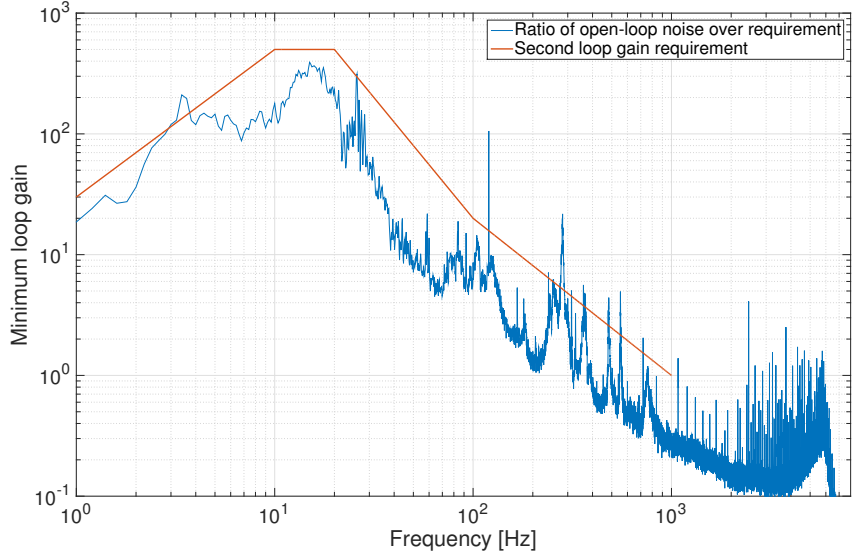


Figure 7: Requirements on the open loop gain of the ISS second loop. Blue trace is the minimum requirement, given by the ratio of the measured noise with open loop and the RIN requirement. The orange trace is the proposed open loop gain.

Poles [Hz]	Zeros [Hz]
0.07	3.1
0.07	3.6
2681	130
8721	2315

Table 1: List of poles and zeros for the whole plant (actuation and IMC pole) as seen by the ISS second loop, measured in W in transmission of the IMC over ISS second loop control signal. The gain at 20 Hz is 0.004 W/V. Fig. 8 shows the Bode plot of this plant (without the IMC pole).

The control topology of the second loop is described in details in [1]. The output signal from the second loop servo board is added to the error signal of the first loop. The bandwidth of the first loop is much higher than the target bandwidth for the second loop, so in first approximation we can consider the first loop gain as infinite. This means that the output signal of the second loop servo is in units of the error signal of the first loop. However, the second loop output is added to the first loop error point after the signal conditioning (whitening) electronics of the first loop. So the actuator response, as seen from the second loop, is determined by the transimpedance and the signal conditioning of the first loop. Figure 8 shows the modeled actuation response (one over the first loop transimpedance and the whitening filter) in units of laser power before the IMC over the second loop control signal, valid only inside the bandwidth of the first loop, so below few kHz. In addition one should consider the IMC pole at about 8.7 kHz. Table ?? lists the poles and zeros of the complete plant response, including the IMC pole

In the present implementation of the ISS second loop, the shape of the first loop whitening was somehow compensated by the second loop whitening, even though the shape was not exactly the

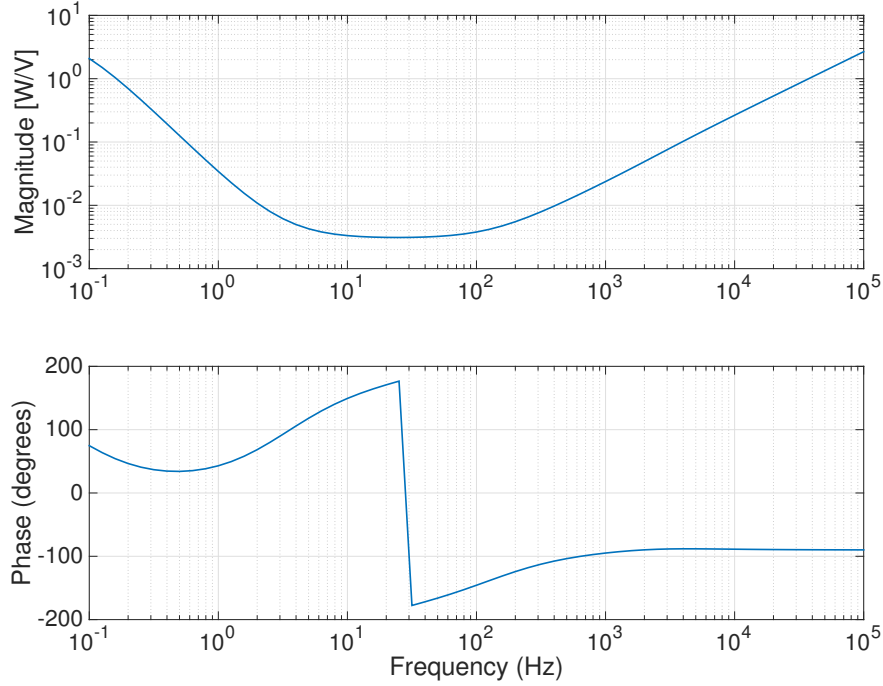


Figure 8: Model of the actuator response, as seen from the ISS second loop output signal. This model is valid only below the unity gain frequency of the first loop servo (few kHz).

same. We suggest to implement a signal conditioning filter in the new second loop servo electronics that matches exactly the one in the first loop whitening, to simplify the control loop design.

It is desirable to be able to adjust the servo gain over a wide range (40 dB as in the present electronics) and to have additional stages of low frequency boosts that can be switched on and off smoothly. We suggest to include an overall variable gain of 40 dB, and three switchable stages. In the present implementation we have: a low frequency boost, an integrator, and an additional gain of 20 dB.

A block diagram of the servo electronics is shown in fig. 9.

4.2 AS vs. DC coupling

The current implementation of the second loop servo is DC coupled. This means that the servo needs an additional input in the form of a low passed offset that is subtracted from the error signal. In the operation of the ISS second loop at LHO, setting this offset proved to be quite difficult. The ISS inner loop (stabilization on the PSL table) is also DC coupled, so a wrong offset in the second loop will offset the inner loop.

For some time the solution to this issue was the implementation of a switch on script with the Guardian infrastructure. With the ISS second loop on at the lowest possible gain, but with the

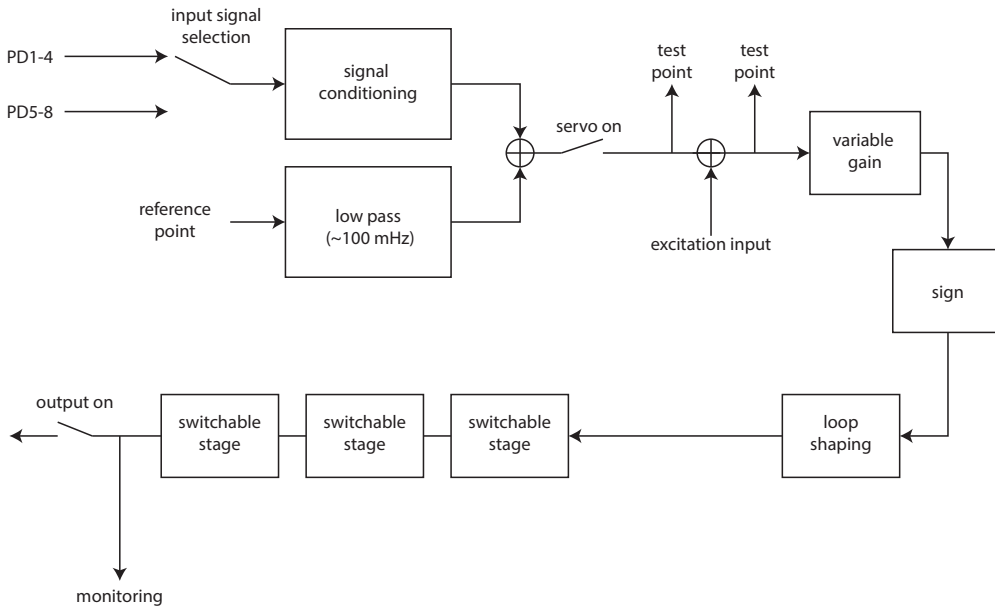


Figure 9: Block diagram of the proposed second loop servo electronics.

output disconnected from the actuation point, the input offset was adjusted to bring the output close to zero. Then the ISS second loop output was enabled and the gain increased to the maximum. To avoid drifting of the ISS inner loop control signal (diffracted power of the AOM) a slow Guardian servo was implemented to keep the diffracted power constant.

This solution worked fine, until some changes in the IMC state increased a lot the low frequency (3 Hz) fluctuations of the power transmitted by the IMC. Such fast fluctuation could not be dealt with by the slow guardian servo, so the ISS second loop engagement became problematic during the last part of O1.

A proposed solution was to make the second loop AC coupled, and get rid of the input offset. This would simplify the engagement of the ISS second loop, but it is not a viable solution to overcome the problems created by the 3 Hz RIN fluctuations. Indeed it is not feasible to have a gain of about 500 at 10 Hz and decouple the loop at 3 Hz.

Our suggestion is to maintain the current implementation: **a DC coupled loop with an input offset. A digital "AC coupling" can be implemented using the real time model instead of the guardian.** This solution has already been successfully tested at LHO [14]. The PSL real time model implements a servo with 0.8 Hz bandwidth to keep the ISS output close to zero before engagement; the output is switched on with a zero crossing logic; after the loop is engaged, the input offset is slowly servoed to maintain a constant diffracted power.

It's been suggested to implement a switchable low pass filter in the reference point input: in this way we can have a 10 Hz low pass during lock acquisition, and later switch on to a much more aggressive low pass, like the 100 mHz.

References

- [1] Jan Hendrik Pöld, Peter King, Benno Willke, *Control loop design for the aLIGO second loop power stabilization*, T1300867-v1
- [2] P. King, *Outer Loop Power Stabilisation Final Design*, T1100265-v1
- [3] R. Martin, L. Williams, J. Gleason, R. Savage, G. Mueller, *Mode Matching to ISS-PD*, T1400176-v1
- [4] E. Sanchez, L. Williams, *ALIGO IO PSL ISS PD ASSEMBLY*, D1101059-v5
- [5] P. King, *Second Loop ISS Transimpedance Amplifier*, D1300639-v1
- [6] J. H. Pöld, *aLIGO PSL ISS second loop servo*, D1300493-v2
- [7] S. Karki, *Comment to LHO elog 20394*,
<https://alog.ligo-wa.caltech.edu/aLOG/index.php?callRep=20394>
- [8] MIST v1.7.0, <http://sourceforge.net/projects/optics-mist/>
- [9] GWINC v3, <https://awiki.ligo-wa.caltech.edu/aLIGO/GWINC>
- [10] V. Frolov, D. Martinov, LLO elog 13767
<https://alog.ligo-la.caltech.edu/aLOG/index.php?callRep=13767>
- [11] G. Vajente, LLO elog 14091
<https://alog.ligo-la.caltech.edu/aLOG/index.php?callRep=14091>
- [12] D. Martinov, LLO elog 14736
<https://alog.ligo-la.caltech.edu/aLOG/index.php?callRep=14736>
- [13] G. Vajente, LHO elog 20534
<https://alog.ligo-wa.caltech.edu/aLOG/index.php?callRep=20354>
- [14] K. Izumi, LHO elog 25316 and 25358
<https://alog.ligo-wa.caltech.edu/aLOG/index.php?callRep=25316>
<https://alog.ligo-wa.caltech.edu/aLOG/index.php?callRep=25358>
- [15] E. Hall, LHO elog 23350
<https://alog.ligo-wa.caltech.edu/aLOG/index.php?callRep=23350>